Dehydrocoupling of dimethylamine borane by titanocene: Elucidation of ten years of inconsistency between theoretical and experimental descriptions.

Jingwen ZHU, [†] Emilie-Laure ZINS, [†] and Mohammad Esmail ALIKHANI [*†]

[†] Sorbonne Université, CNRS, De la Molécule aux Nano-Objets: Réactivité, Interactions Spectroscopies, MONARIS, 75005, Paris France

[*] Corresponding Author:

esmail.alikhani@sorbonne-universite.fr

Abstract

More than ten years ago, Manners and coworkers published the first experimental study on the efficiency of titanocene to catalyze the dehydrocoupling of dimethylamine borane (DMAB, *JACS* 2006, *128*, 9582). Several experimental investigations have shown that a two-step mechanism leads to the formation of a cyclic diborazane $(Me_2N\text{-}BH_2)_2$ *via* the linear diborazane ($HNMe_2\text{-}BH_2\text{-}NMe_2\text{-}BH_3$). This finding stood in contradiction with following theoretical investigations of the reaction pathway. Herein, using dispersion-corrected density functional theory (DFT-D), we propose an energetically favored reaction mechanism in perfect agreement with the experimental findings. It is shown that van der Waals interactions play a prominent role in the reaction pathway. The formation of 3-center 2-electron interactions, classical dihydrogen bonds, as well as non-classical dihydrogen bonds, was identified with the help of topological and localized orbital approaches.

Introduction

The dehydrocoupling reactions between main group elements are currently the subject of numerous studies in organometallic synthesis laboratories.[1-3] These reactions result in the synthesis of new inorganic compounds in particular new polymers with varied properties. Since these reactions lead to the elimination of dihydrogen, they are also studied for possible applications in the elaboration of hydrogen storage material.[4,5]

The study of the catalytic dehydrocoupling of amine-boranes fits perfectly in this double context of generation of high added-value products such as white graphene, and the controlled release of dihydrogen.[6-9]

Organometallic catalysis has proved particularly well suited to promote and control the dehydrogenation of dimethylamine borane (DMAB).[10-14] In addition, Group IV metallocenes have been among the most used catalysts for more than 30 years due to their easy synthesis and use. Since titanium is the second most abundant transition metal on Earth, titanocene can be considered as a green catalyst in a sustainable economy.[15]

It is probably all these reasons that explain the numerous studies carried out on the dehydrogenation of DMAB by titanocene. In 2006, Manners' team studied experimentally this reaction for the first time.[16] They have outlined the efficiency of this catalyst for the dehydrocoupling of both DMAB and diisopropylamine borane (D^iPrAB) and demonstrated that the dehydrocoupling of DMAB involves a homogeneous catalyst and leads to the formation of a cyclic diborazane $(Me_2N\text{-}BH_2)_2$, with the loss of two dihydrogen molecules. However, for more sterically encumbered substrates, such as D^iPrAB, the aminoborane $^iPr_2N{=}BH_2$ is the final product of the dehydrogenation reaction.

Taking up the challenge, Luo and Ohno[17] studied the reaction pathways leading to the catalytic dehydrogenation of DMAB using density functional theory (DFT), with the B3LYP functional. They proposed two possible reaction pathways: (i) a first process involving a single molecule of DMAB (intramolecular mechanism) resulting in the formation of the aminoborane $Me_2N{=}BH_2$, and (ii) a second, intermolecular process involving two DMAB molecules leading to the formation of the linear dimer. From their calculated potential energy surfaces, they concluded that the intramolecular mechanism was the preferable pathway compared to the intermolecular one. To come to an agreement with the experimental finding, they suggested a further off-metal dimerization of the $Me_2N{=}BH_2$ species, leading to the formation of the cyclic diborazane.

Three years later, Manners et al.[18] published out an extensive experimental study to elucidate the reaction mechanism of titanocene-catalyzed dehydrogenation of amine-boranes. In the case of the dehydrogenation of DMAB, their study has highlighted the role of the $HNMe_2$-BH_2-Me_2N-BH_3 linear diborazane as a reaction intermediate prior to the formation of the cyclic diborazane $(Me_2N\text{-}BH_2)_2$. They also demonstrated that this dehydrogenation process involves two consecutive catalytic cycles:

- At first, they proposed a two-step cycle leading to a coordination complex $[Cp_2Ti(\eta^2\text{-}BH_3{\cdot}NHMe_2)]$ involving a 3-center 2-electron (3C/2e) Ti-H-B interaction. This complex further undergoes a proton transfer. When adding a second molecule of DMAB, another two-body reaction is expected to lead to the formation of the linear dimer, with the concomitant loss of one H_2 molecule.
- The second cycle consists in the dehydrocoupling of the linear dimer resulting in the cyclic diborazane upon Cp_2Ti catalytic process.

In 2013, Tao and Qi reinvestigated the reaction pathway of the catalytic dehydrocoupling of the DMAB within the DFT framework.[19] Their conclusion was fully in line with the previous theoretical work and again, at odds with the experimental finding.

Thus, despite two theoretical investigations, the dehydrocoupling mechanism of DMAB catalyzed by titanocene remains incompletely understood. The inconsistency between theoretical and experimental results is summarized in Scheme 1.

Scheme 1: DMAB dehydrocoupling mechanism from both experimental (Exp.)[1,18] and theoretical (DFT)[17,19] points of view.

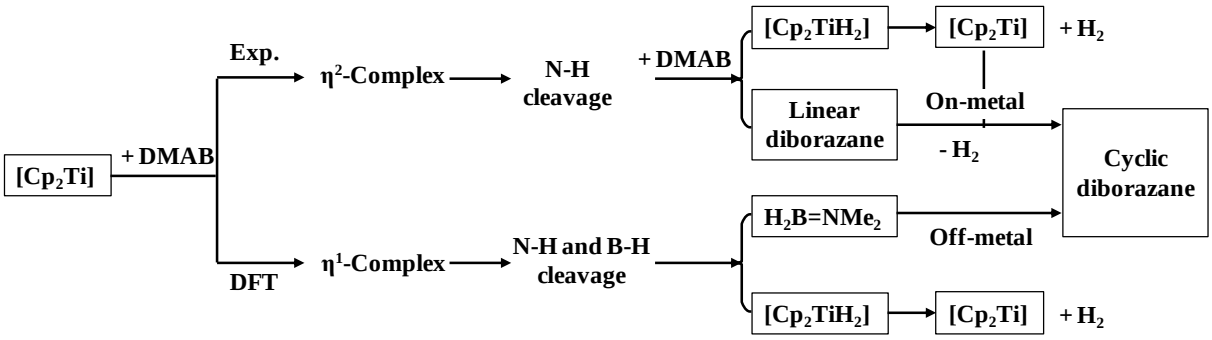

This inconsistency has also been highlighted in two recent reviews on the catalyzed dehydrogenation of amine boranes, by Weller et al.[8] and Rossin and Peruzzini.[20] Understanding the full mechanism would be an essential step towards an improvement in tailoring processes establishing new chemical bonds between p-block elements, with concomitant loss of H_2. The present study aims at re-investigating these reaction pathways

combining density functional theory (DFT) and interpretative methods. To this end, we reconsider the previously proposed mechanisms using the dispersion-corrected density functional theory (DFT-D) that enables a much suitable description of non-covalent interactions.[21] A detailed electronic and bonding description of each compound involved in the reaction path will be performed within the topological frameworks. We will pay a particular attention to the effects of non-covalent interactions on the bond-formation/dissociation process along the reaction.

Computational methods

All calculations were performed using the Gaussian 09 Rev D.01 quantum chemical package.[22] The geometrical structures at all stationary points were fully optimized with the popular three-parameter functional B3LYP, to which has been added the so-called Grimme empirical dispersion correction with Becke-Johnson damping (GD3BJ).[23,24] This functional is referred to as B3LYP-GD3BJ in the following. There are two main reasons for the choice of this functional: first, the reliability of this functional to describe the non-covalent interactions,[25,26] and second, to facilitate comparisons with the previous theoretical works[17,19] which used the same, B3LYP functional. All optimizations were undertaken with the same basis set as the one used in the Luo and Ohno's theoretical work: 6-31G* for cyclopentadienyl (Cp) and methyl groups, 6-31++G** for all the atoms involved in the bond-formation/dissociation, and the LanL2DZ relativistic pseudo-potential for the metal atom. Vibrational frequency calculations have been performed to obtain the ZPE (vibrational zero-point-energy) as well as Gibbs free energies and to check the nature of the stationary point (minimum or transition state, TS).

The effect of solvent in energy was investigated along the reaction pathways by performing calculations with the PCM (Polarizable continuum) model[27] and taking toluene as solvent.

Bonding characterization was discussed using both the Electron localization Function (ELF) [28 - 30] and Quantum Theory of Atoms In Molecules (QTAIM) [31 , 32] topological frameworks with the TopMod[33] and AIMAll[34] softwares, respectively. In addition, an orbital analysis has been done with the NBO 6.0 program on the optimized geometry.[35]

In order to check our theoretical results obtained with the B3LYP-GD3BJ functional, we performed a single point calculation using the high level ab initio CCSD(T)[36,37] method on the optimized geometry of the first η^1- and η^2-complexes formed in the entrance channel of the $Cp_2Ti + H_3B\text{-}NHMe_2$ reaction.

Results and discussion

1 – The [$Cp_2Ti(BH_3{\cdot}NHMe_2)$] adduct: a 3-center 2-electron species

In the entrance channel, the two-body interaction between one Cp_2Ti and one DMAB molecule may lead to the formation of two different σ complexes, in which one or two hydrogen atoms of the BH_3 moiety interact *via* a 3-center 2-electron (3C/2e) bonding motif with Ti center. In Figure 1 are reported some relevant geometrical parameters for both adducts.

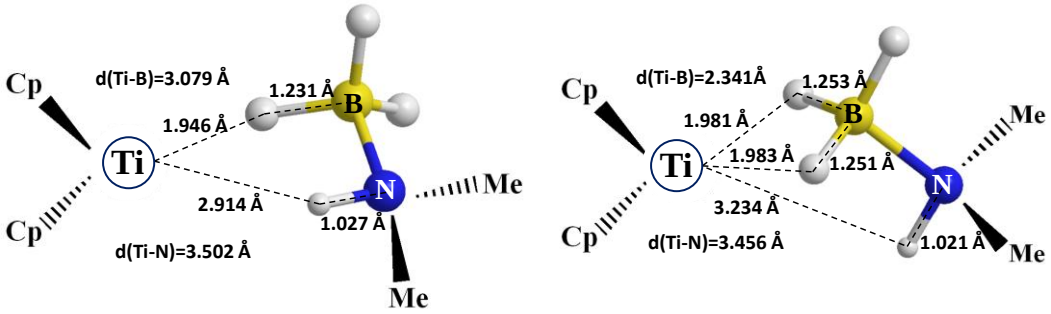

[$Cp_2Ti(\eta^1\text{-}BH_3{\cdot}NHMe_2)$] **[$Cp_2Ti(\eta^2\text{-}BH_3{\cdot}NHMe_2)$]**

Figure 1: Some important geometrical parameters of the [$Cp_2Ti(BH_3{\cdot}NHMe_2)$] complexes.

Both complexes are characterized by a relatively short Ti···H(B) distance (1.946 Å in η^1-complex, and 1.981/1.983 Å in η^2-adduct) and a lengthening of the corresponding B-H bond with respect to the isolated DMAB (1.202 Å). The Ti-B distance is notably shorter in the η^2-complex (2.341 Å) than in η^1-complex (3.079 Å). It is also worth noting that our geometrical parameters are rather close to those obtained with the same B3LYP functional in previous studies.[17,19] Nevertheless, the binding energy calculated with respect to free partners varies much depending on whether or not the dispersion-correction component is included in the B3LYP functional ($\Delta E(\eta^1$-complex) = -33 & -78 kJ/mol and $\Delta E(\eta^2$-complex) = -53 & -104 kJ/mol, for B3LYP and B3LYP-GD3BJ levels respectively). A single-point calculation at the CCSD(T) level on the structures optimized at the B3LYP level gives a similar binding energy to that obtained with B3LYP-GD3BJ ($\Delta E(\eta^1$-complex) = -76 and $\Delta E(\eta^2$-complex) = -105 kJ/mol). Consideration of the energy difference between B3LYP and B3LYP-GD3BJ results leads to quite contradictory conclusion when Gibbs free energy is taken into account. As shown in Figure 2, both η^1- and η^2-complexes are endoergic at the B3LYP level, while they are exoergic with B3LYP-GD3BJ and CCSD(T) methods.

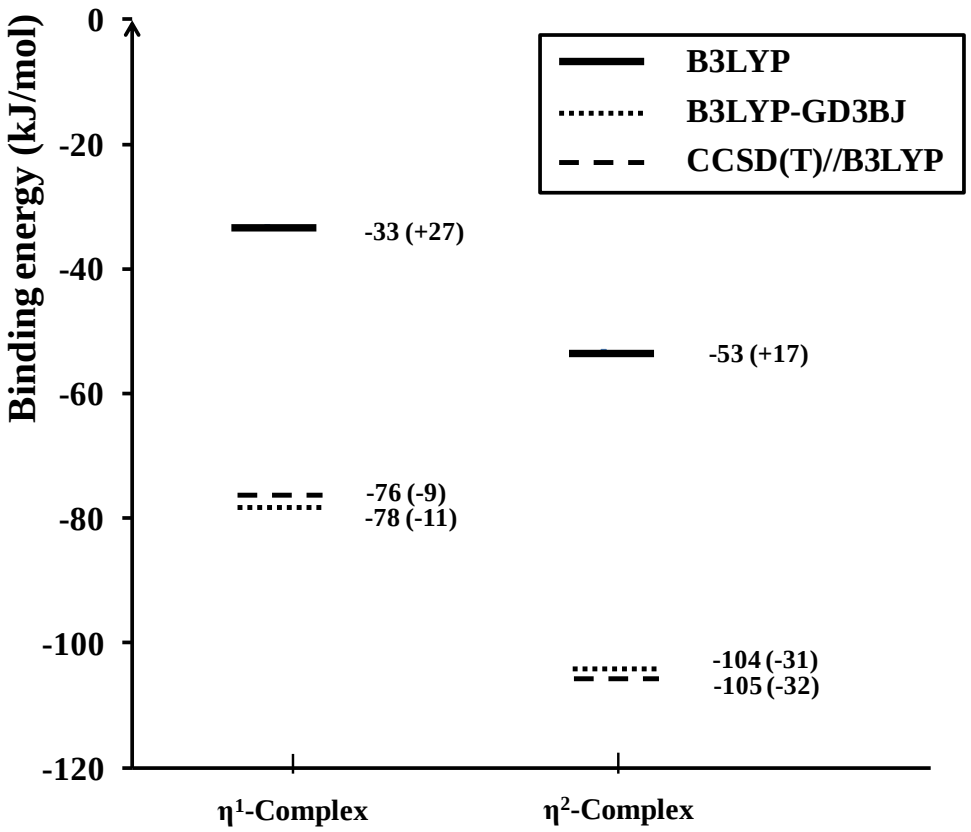

Figure 2: Binding energies (relative Gibbs free energies) calculated at three different levels of theory.

The QTAIM analysis[38] of these complexes reveal one BCP (Bond Critical Point) and one BP (Bond Path) between Ti and one hydrogen atom of BH_3 in the case of the η^1-complex (ρ[BCP(Ti···H)] = 0.039 a.u. and $\nabla^2\rho$[BCP(Ti···H)] = +0.14 a.u.). The ELF topological analysis[39,40] of the protonated V(Ti,B,H) basin clearly shows the presence of a 3C/2e interaction in the η^1-complex (population of basin V(Ti,B,H) = 2.00 e, with 5% for Ti, 13% for B and 82% for H). For the η^2-complex, the close contact between boron and titanium atoms results in the formation of a BCP (ρ[BCP(Ti-B) = 0.055 a.u. and $\nabla^2\rho$[BCP(Ti-B)] = +0.13 a.u.) with high ellipticity ($\approx$ 16) indicating the easy and probable evolution of this point to the formation of two BCP connecting the Ti center to two hydrogen atoms of BH_3. This feature is clearly revealed by the ELF atomic contribution of these two protonated basins. Owing the positive sign of the Laplacian charge density at bond critical point, the Ti-H and Ti-B interactions belong to the closed-shell interaction.

2 – Path 1: from the [$Cp_2Ti(\eta^1\text{-}BH_3{\cdot}NHMe_2)$] adduct to the linear diborazane

As illustrated in Figure 3, the initial step of this dehydrogenation reaction starts with a formation of the two-body η^1-complex (labelled as S_1) which proceeds, *via* a low barrier height (≈ 20 kJ/mol), to an N-H oxidative addition at the Ti center, forming the [$Cp_2TiH{:}H_3B\text{-}NMe_2$] species (labelled as S_2 in Figure 3) with a large stabilization energy (≈ 100 kJ/mol). Two bond critical points are characterized for this intermediate: a BCP located between Ti and N atoms and another between Ti and H of BH_3 subunit. The former indicates the formation of a Ti-N bond with ρ[BCP(Ti-N)] = 0.059 a.u. and ∇^2ρ[BCP(Ti-N)] = +0.17 a.u.. The second BCP is characteristic of a 3C/2e interaction (ρ[BCP(Ti···H)] = 0.064 a.u. and ∇^2ρ[BCP(Ti···H)] = +0.13 a.u.).

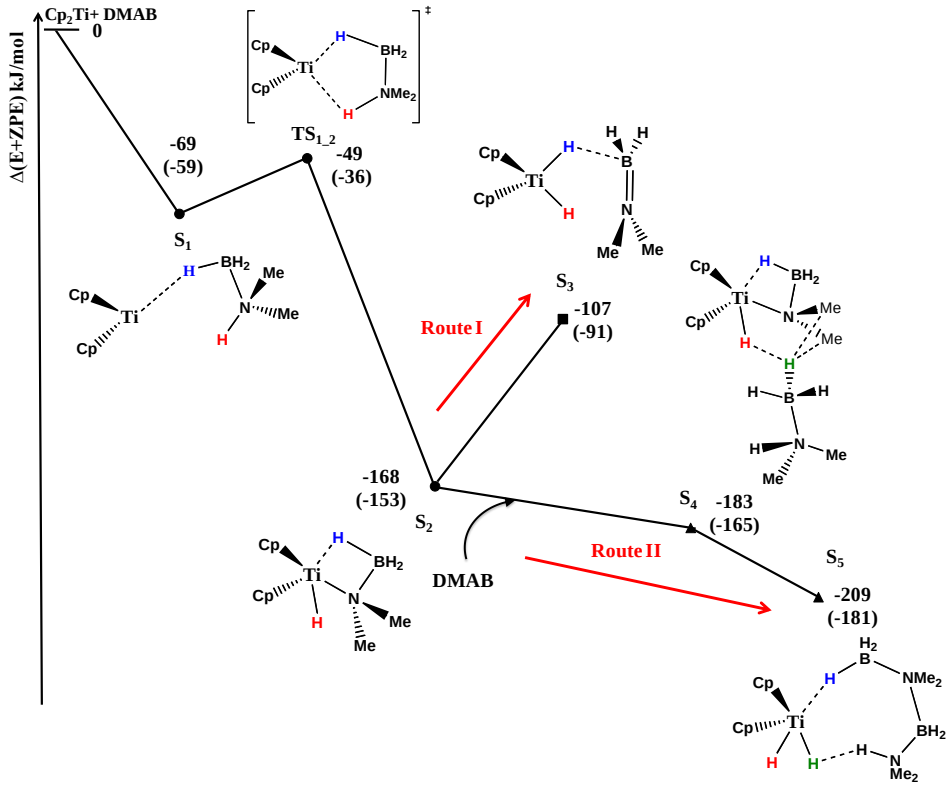

Figure 3: Energy profile along the first reaction pathway. Relative gas-phase zero-point corrected energies and solvent effect-corrections (values in parentheses) are given in kJ/mol.

The S_2 intermediate can further undergo an endothermic step with an energy of about 61 kJ/mol to generate a two-body complex formed between Cp_2TiH_2 and $H_2B{=}NMe_2$ (labelled as S_3 corresponding to Route I in Figure 3). Weak intermolecular interactions are responsible to the formation of this complex.

Competitively, we could consider at this stage a second step toward the dehydrocoupling of DMAB. Addition of a second DMAB molecule to the S_2 intermediate indeed leads to the formation of a new complex (labelled as S_4 in Figure 3). This alternative reaction path (Route II in Figure 3) goes actually downhill with a small energy gain of about 15 kJ/mol. Consequently, the Route II is energetically more favorable than the Route I. To the best of our knowledge, the S_4 complex is optimized here for the first time along the dehydrogenation path of DMAB by Cp_2Ti. It should be noted that the optimized S_4 complex is actually a good candidate for the hypothetical structure suggested by R. Waterman in a comprehensive review[41] in 2013 to explain and complement the Manners' mechanistic model.

The QTAIM analysis of the bonding pattern in the S_4 complex clearly reveals the formation of a dihydrogen bond-like interaction (Figure 4), with ρ[BCP(H⋯H)] = 0.005 a.u. and $\nabla^2\rho$[BCP(H⋯H)] = +0.01 a.u. between the second DMAB molecule and the hydrogen atom directly linked to the Ti center. However, a thorough charge analysis demonstrates that the net atomic charge borne by each of the two hydrogen atoms engaged in the H⋯H interaction is negative, q(H(B)) = -0.68 e and q(H(Ti))= -0.34 e. As a consequence, this interaction could be labelled as $X\text{-}H^{\delta-}\cdots^{\delta-}HML_n$, unlike in a classical dihydrogen bond that correspond to $X\text{-}H^{\delta+}\cdots^{\delta-}H\text{-}Y$ pattern.[42] The concept of "homopolar dihydrogen bond", expressed as $X\text{-}H^{\delta-}\cdots^{\delta-}H\text{-}X$ or $X\text{-}H^{\delta+}\cdots^{\delta+}H\text{-}X$, is a well-known concept for B-H⋯H-B or C-H⋯H-C interactions.[43-45] It drew the attention of researchers, because of the dominant role of van der Waals attractive interactions rather than the classical electrostatic interactions in the stabilization of the intermediate complexes. However, the kind of interaction identified in S_4 appears to be slightly different. To the best of our knowledge of the literature, this is the first identification of an $X\text{-}H^{\delta-}\cdots^{\delta-}HML_n$ homopolar dihydrogen bond. Other dihydrogen bonds are also identified in this intermediate. B-H··H-C interactions between the BH_3 moiety and methyl groups or Cp ligands (which are not presented in Figure 4) have electron density in the [0.004 a.u., 0.006 a.u.] ranges.

From S_4 one, the formation of the precursor of the linear dimer and titanium hydride (S_5) is an exothermic process, which releases approximately 25 kJ/mol. The formation of this intermediate involves the cleavage of the Ti-N bond and a concerted Ti-H-B-N ring opening process. Concomitantly, as shown in Figure 4, the electron density at BCP(Ti⋯H) decreases from 0.063 to 0.036 a.u. in going from S_4 to S_5. An ELF atomic contribution showed that the Ti⋯H bonding should be considered as a 3C/2e interaction (V(Ti,B,H) = 1.93 e, with 3% for Ti, 13% for B and 84% for H). Furthermore, a dihydrogen bond is identified in S_5 (labelled as

BCP(H···H) in Figure 4), in which the net atomic charge of the hydrogen atoms are of opposite signs. The electron density at this bond critical point amounts to 0.045 a.u., slightly larger than that of the Ti···H 3C/2e bond.

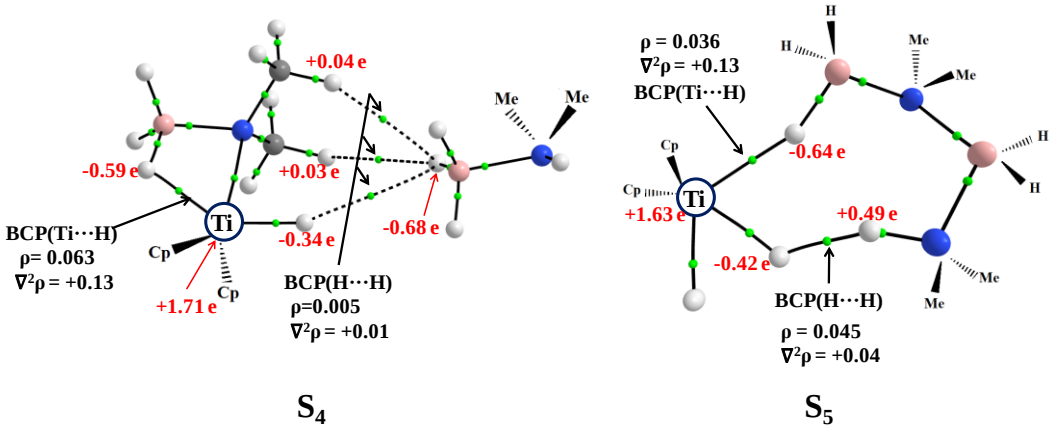

Figure 4: Bond Critical Points and AIM atomic charges in S_4 and S_5 complexes.

In line with the outcomes of the discussion on the energy profile along the reaction path 1, we could therefore suggest a full mechanistic cycle for the catalytic formation of a linear diborazane and release of an equivalent H_2 (Figure 5). The suggest mechanism is in agreement with the experimental scheme proposed by Manners' team.[18]

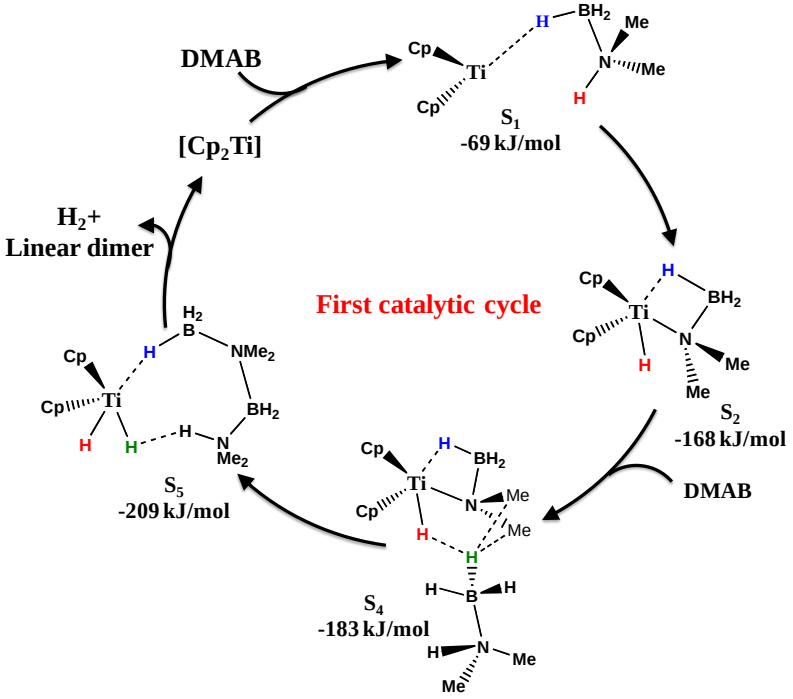

Figure 5: First catalytic cycle from $[Cp_2Ti(\eta^1\text{-}BH_3{\cdot}NHMe_2)]$ adduct to linear diborazane *via* a dihydrogen-bonded complex. Relative energies calculated in the gas-phase including ZPE correction in kJ/mol are mentioned.

3 – Path 2: From the [$Cp_2Ti(\eta^2\text{-}BH_3{\cdot}NHMe_2)$] adduct to the linear diborazane

Such a catalytic cycle involving a three-body interaction was already proposed in one of the previous theoretical work,[17] but had been ruled out, because of an endoergic reaction in the entrance channel with a high barrier height (≈ 130 kJ/mol) at the B3LYP level of theory.

In the present work, owing to the use of the dispersion-corrected DFT approach, this path has been calculated to be both energetically and kinetically favorable. As show in Figure 6, the first step corresponds to the formation of a three-body complex, consisting of an η^2-complex and the addition of a second DMAB to the η^2-complex, leading to a new complex with a binding energy about 164 kJ/mol (labelled as S_6 in Figure 6).

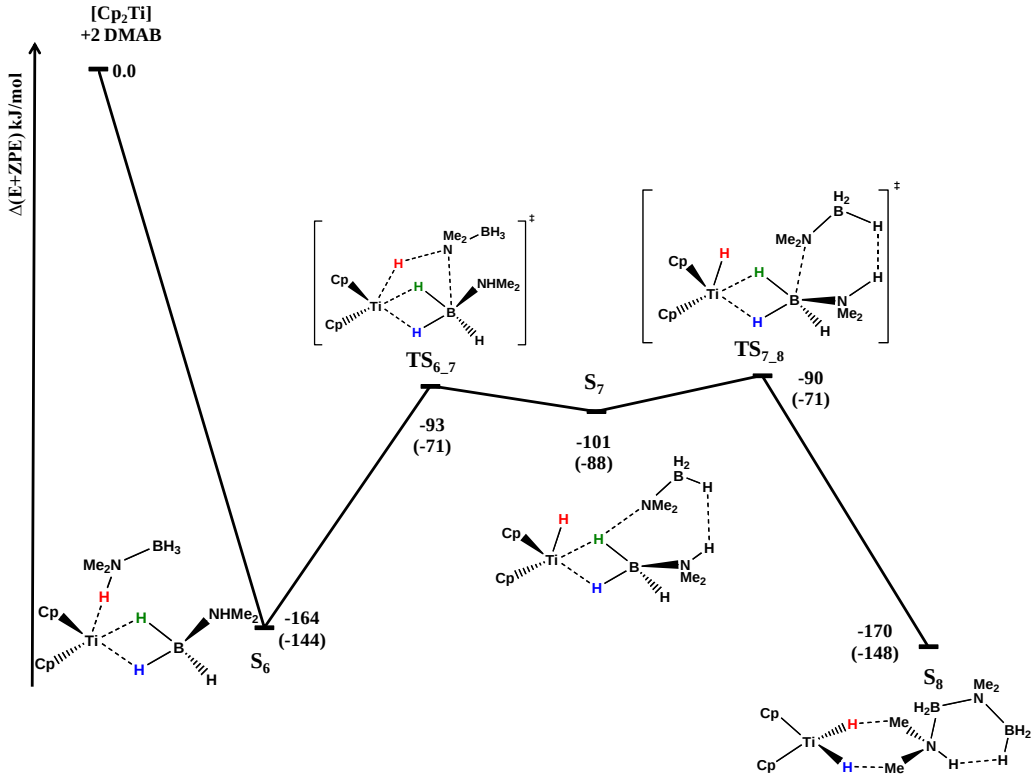

Figure 6: Energy profile along the second reaction pathway. Relative gas-phase zero-point corrected energies and solvent effect-corrections (values in parentheses) are given in kJ/mol.

From the QTAIM analysis of the S_6 complex, a weak intermolecular interaction is identified between the titanium atom (q(Ti) = +1.34 e) and the hydrogen atom (q(H(N)) = +0.44 e) linked to the nitrogen atom of the second DMAB molecule (ρ[BCP(Ti···H-N)] = 0.017 a.u. and $\nabla^2\rho$[BCP(H···H-N)] = +0.01 a.u.). The ELF analysis of the atomic contributions on the corresponding protonated basin clearly shows that the present interaction could not be considered as a 3C/2e one. We further investigated the nature of the interaction by means of

the NBO (Natural Bond Orbital) analysis, which provides a measure of the electron donor-acceptor delocalization.[46] As illustrated in Figure 7, this interaction should be considered as a donor-acceptor interaction from a lone pair orbital of titanium (d_{z^2}) toward an anti-bonding orbital of N-H (σ*), $d_{z^2}(Ti) \rightarrow \sigma^*(N-H)$ producing a stabilization of 6.3 kcal/mol.

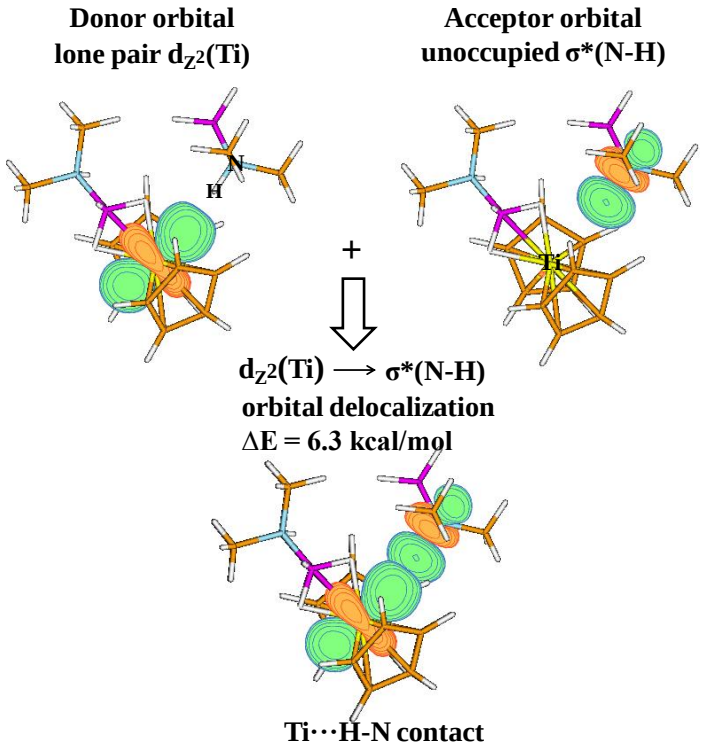

Figure 7: Donor-acceptor interaction in the S_6 complex.

Transformation of S_6 to S_7 is characterized by a hydrogen transfer from the nitrogen atom to the metal center, which leads to the formation of titanium hydride. From energetic point of view, the S_7 intermediate evolves towards a new complex (labelled as S_8 in Figure 6) without any energy demand. In the latter complex, dihydride titanium interacts with the linear diborazane fragment *via* two dihydrogen bonds (ρ[BCP(Ti-H···H-C)] = 0.011 a.u. and ∇^2ρ[BCP(Ti-H···H-C)] = +0.03 a.u.). As illustrated in Figure 8, we identified three bond critical points at the N-B bonds with electron density of 0.122, 0.140, and 0.122 a.u.. It is interesting to note the presence of a dihydrogen bond (labelled as N-H···H-B in Figure 8) in the linear diborazane fragment (ρ[BCP(N-H···H-B)] = 0.032 a.u.), which seems to be the likely cause of the closing of the six-membered ring in a chair-like conformation.

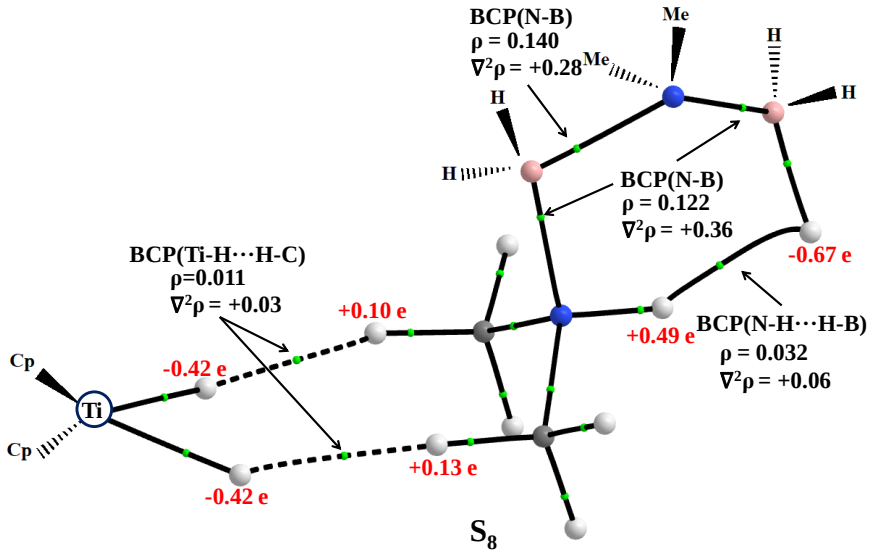

Figure 8: Bond Critical Points and AIM atomic charges in S_8 complex.

Accordingly, this three-body mechanism beginning with the $[Cp_2Ti(\eta^2\text{-}BH_3{\cdot}NHMe_2)]$ adduct is calculated to be energetically similar to the first catalytic cycle induced by the formation of the $[Cp_2Ti(\eta^1\text{-}BH_3{\cdot}NHMe_2)]$ adduct. Thus, within the DFT-D framework, two competitive reaction pathways are found to lead to the linear diborazane intermediate that should further undergo an "on-metal" cyclization, according to the experimental findings.

4 – Path 3: From the linear diborazane to the cyclic diborazane

Experimental data demonstrated that the cyclization of the linear diborazane is a heterogeneously catalyzed process. We thus computationally investigated an "on-metal" cyclization of the linear dimer. The calculated energy profiles of this reaction pathway are presented in Figure 9. A similar mechanism was already investigated by Tao and Qi at the DFT level.[19] Their results suggested that this mechanism is highly endothermic. On the contrary, our results obtained within the DFT-D framework demonstrate that this dehydrocoupling pathway is an energetically feasible process under the experimental conditions (Figure 9). This reaction pathway involves three intermediates, named S_9, S_{10} and S_{11}, as well as two transition states, named TS_{9_10} and TS_{10_11}.

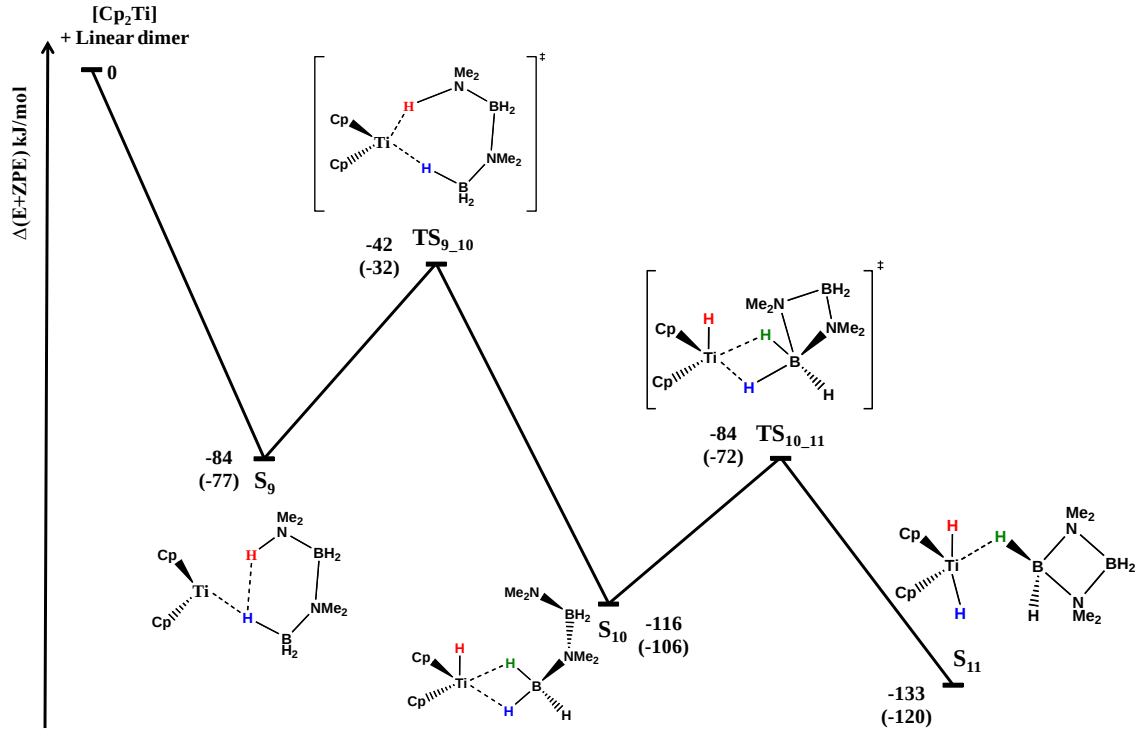

Figure 9: Energy profile for the titanocene-catalyzed dehydrocoupling of linear diborazane. Relative gas-phase zero-point corrected energies and energies taking into account of solvent effect (values in parentheses) are shown in kJ/mol.

The cyclization process first involves the coordination of the linear diborazane molecule to the metal center with a binding energy of -84 kJ/mol (S_9 intermediate). An η^1 3C/2e intermolecular interaction is identified in this S_9 intermediate, thanks to the Bader's analysis, with a ρ[BCP(Ti···H(B))] value of 0.046 a.u. and the ELF analysis confirms the 3C/2e nature of this interaction (V(Ti,B,H) = 1.99 e, with 4% for Ti, 13% for B and 83% for H). It is interesting to note that an intramolecular dihydrogen-bond is identified between the protic N-$H^{\delta+}$ hydrogen and the hydride-like $^{\delta-}$H-B end with ρ[BCP(N-H···H-B)] value of 0.021 a.u., slightly smaller than its counterpart in S_8 (0.032 a.u., Figure 8).

Over the low barrier height, the cleavage of the N-H bond leads to a new intermediate (labelled as S_{10} in Figure 9), in which we note an asymmetric η^2 3C/2e interactions between the titanocene and the amidoborane fragment, characterized by two distinct BCPs (ρ = 0.056 and 0.062 a.u.). The catalytic cycle is completed with a second hydrogen transfer from borane to the metal center, producing the so-called cyclic diborazane (labelled as S_{11} in Figure 8). The QTAIM and ELF analyses suggest that the cyclic diborazane is connected to the dihydride titanocene *via* a 3C/2e interaction (ρ = 0.037 a.u., V(Ti,B,H) = 1.97 e, with 3% for Ti, 15% for B and 82% for H) and five weaker dihydrogen bonds (0.004 < ρ < 0.008 a.u.).

As interim first conclusion, we summed up the three paths studied above in Scheme 2, which consistently allowed us to describe and complement the experimental considerations.

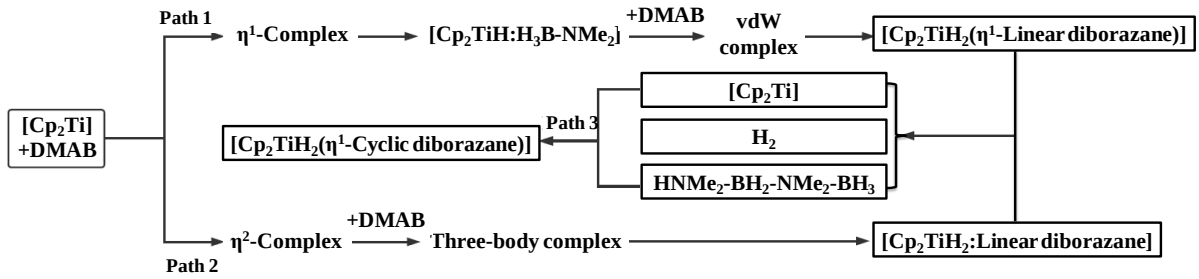

Scheme 2: A bridged schematic representation of the catalytic formation of the cyclic diborazane.

5 - Substitution effect on the terminal product

Experimental investigations also showed a fundamentally different reaction path in case of a bulky substituant on the nitrogen, such as diisopropylamine borane (D^iPrAB). Indeed, the dehydrocoupling of the D^iPrAB leads to the formation of the so-called aminoborane $^iPr_2N{=}BH_2$ product. Our computational results enable us to explain the singularity of D^iPrAB dehydrogenation path in two ways.

First, a careful look to the energetics reported in Figure 10 reveals that in contrast to the case of DMAB, the "Route I" transforming the S_2 structure to the aminoborane (S_3) is more favorable than the "Route II" for the D^iPrAB.

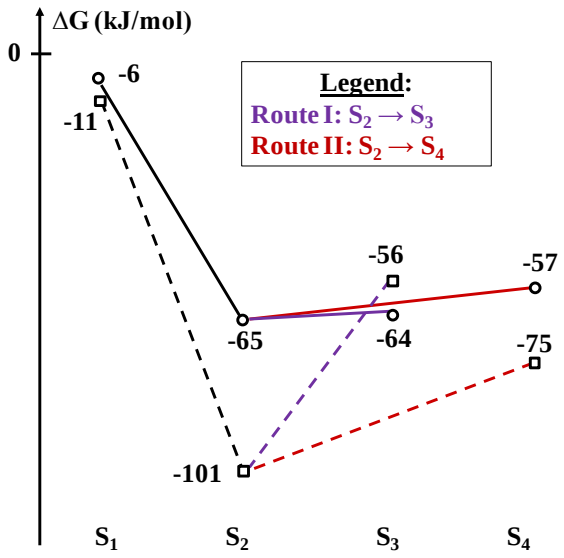

Figure 10: Relative Gibbs free energy of four structures along the path 1 (see Figure 3) for both DMAB (full squares, dotted lines) and D^{i}PrAB (full circles, full lines) compounds.

Secondly, as shown in Figure 11, we observe a strong deformation of the vdW complex (S_4) due to the steric hindrance leading to a B···N distance larger than 6 Å, very close to the N···N distance (6.2 Å).

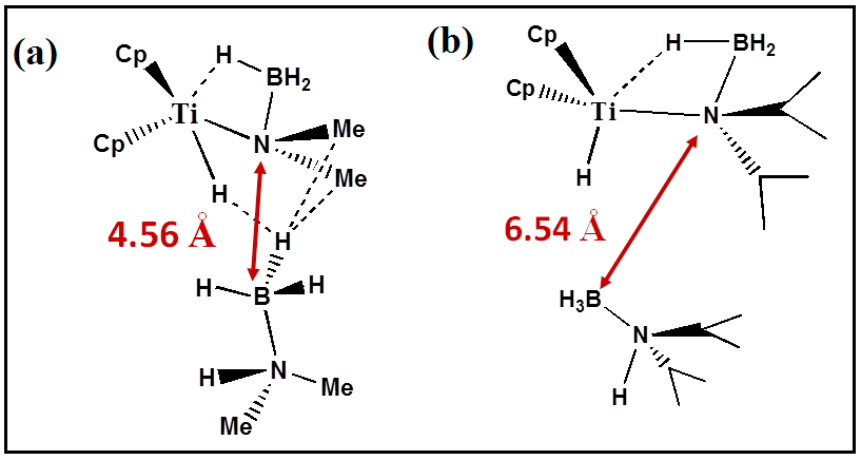

Figure 11: Optimized structure of van der Waals complex labelled as S_4 with (a) DMAB and (b) D^{i}PrAB compounds.

In addition with the geometrical parameters reported in Figure 11, we would like to mention that in the S_4 compound, we identified several dihydrogen bonds between bulky groups of two D^{i}PrAB units, while the dihydrogen bonds observed with DMAB molecules were found between the borane part of the second DMAB and the NMe_2 subunit of the amidoborane. Every dihydrogen bond only presents a low electron density (≈ 0.005 a.u.) at the identified bond critical points for both DMAB and D^{i}PrAB complexes.

Consequently, the dehydrogenation of sterically bulky groups at amine results in the formation of aminoborane rather than diborazane.

Conclusion

Theoretical calculations within the DFT-D framework make it possible to obtain a reaction pathway in perfect agreement with the experimental data: the cyclization of the intermediate occurs *via* an "on-metal" mechanism. A major conclusion of this study is that the formation of a van der Waals complex in which a second DMAB molecule interacts with amidoborane subunit *via* dihydrogen bonds appears to play a central role in the formation of the linear dimer intermediate. The topological (ELF and QTAIM) and orbital (NBO) analyses allowed

us to characterize the natures of non-covalent interactions in the reaction intermediates. Noticeably, we underlined the important role played by weak interactions, such as dihydrogen bonds and 3C/2e interactions, along the catalyzed dehydrocoupling process of DMAB. For a consistent description of these interactions, the coverage of dispersion contribution is fundamental.

Finally, it was also shown that the bulky substituents, as in the $D^{i}PrAB$, prevents the formation of a van der Waals complex leaving open only the path to the formation of a diisopropyl aminoborane.

---

1 Clark, T.; Lee, K.; Manners, I. *Chem. Eur. J.* **2006**, *12*, 8634-8648.

2 Leitao, E.; Jurca, T.; Manners, I. *Nat. Chem.* **2013**, *5*, 817-829.

3 Melen, R. *Chem. Soc. Rev.* **2016**, *45*, 775-788.

4 Crabtree, G.; Dresselhaus, M. *MRS Bulletin* **2008**, *33*, 421-428.

5 Scipioni, A.; Manzardo, A.; Ren, J. *Hydrogen economy*.

6 Staubitz, A.; Robertson, A.; Manners, I. *Chem. Rev.* **2010**, *110*, 4079-4124.

7 Huang, Z.; Autrey, T. *Energy Environ. Sci.* **2012**, *5*, 9257.

8 Johnson, H.; Hooper, T.; Weller, A. *Synthesis and Application of Organoboron Compounds* **2015**, 153-220.

9 Bhunya, S.; Malakar, T.; Ganguly, G.; Paul, A. *ACS Cataltysis* **2016**, *6*, 7907-7934.

10 Jaska, C.; Temple, K.; Lough, A.; Manners, I. *Chem. Commun.* **2001**, 962-963.

11 Pun, D.; Lobkovsky, E.; Chirik, P. *Chem. Commun.* **2007**, 3297.

12 Kawano, Y.; Uruichi, M.; Shimoi, M.; Taki, S.; Kawaguchi, T.; Kakizawa, T.; Ogino, H. *J. Am. Chem. Soc.* **2009**, *131*, 14946-14957.

13 Stevens, C.; Dallanegra, R.; Chaplin, A.; Weller, A.; Macgregor, S.; Ward, B.; McKay, D.; Alcaraz, G.; Sabo-Etienne, S. *Chem. Eur. J.* **2011**, *17*, 3011-3020.

14 Vance, J.; Schäfer, A.; Robertson, A.; Lee, K.; Turner, J.; Whittell, G.; Manners, I. *J. Am. Chem. Soc.* **2014**, *136*, 3048-3064.

15 Collins, R.; Russell, A.; Mountford, P. *Appl. Petrochem. Res.* **2015**, *5*, 153-171.

16 Clark, T.; Russell, C.; Manners, I. *J. Am. Chem. Soc.* **2006**, *128*, 9582-9583.

17 Luo, Y.; Ohno, K. *Organometallics* **2007**, *26*, 3597-3600.

18 Sloan, M.; Staubitz, A.; Clark, T.; Russell, C.; Lloyd-Jones, G.; Manners, I. *J. Am. Chem. Soc.* **2010**, *132*, 3831-3841.

19 Tao, J.; Qi, Y. *J. Organomet. Chem.* **2013**, *745-746*, 479-486.

20 Rossin, A.; Peruzzini, M. *Chem. Rev.* **2016**, *116*, 8848-8872.

21 Ryde, U.; Mata, R.; Grimme, S. *Dalton Trans.* **2011**, *40*, 11176.

22 Gaussian 09, Revision **D.01**, Frisch, M.J.; Trucks, G.W.; Schlegel, H.B.; Scuseria, G.E.; Robb, M.A.; Cheeseman, J.R.; Scalmani, G.; Barone, V.; Mennucci, B.; Petersson, G.A.; Nakatsuji, H.; Caricato, M.; Li, X.; Hratchian, H.P.; Izmaylov, A.F.; Bloino, J.; Zheng, G.; Sonnenberg, J.L.; Hada, M.; Ehara, M.; Toyota, K.;

Fukuda, R.; Hasegawa, J.; Ishida, M.; Nakajima, T.; Honda, Y.; Kitao, O.; Nakai, H.; Vreven, T.; Montgomery, J.A., Jr.; Peralta, J.E.; Ogliaro, F.; Bearpark, M.; Heyd, J.J.; Brothers, E.; Kudin, K.N.; Staroverov, V.N.; Kobayashi, R.; Normand, J.; Raghavachari, K.; Rendell, A.; Burant, J.C.; Iyengar, S.S.; Tomasi, J.; Cossi, M.; Rega, N.; Millam, N.J.; Klene, M.; Knox, J.E.; Cross, J.B.; Bakken, V.; Adamo, C.; Jaramillo, J.; Gomperts, R.; Stratmann, R.E.; Yazyev, O.; Austin, A. J.; Cammi, R.; Pomelli, C.; Ochterski, J. W.; Martin, R.L.; Morokuma, K.; Zakrzewski, V.G.; Voth, G.A.; Salvador, P.; Dannenberg, J.J.; Dapprich, S.; Daniels, A.D.; Farkas, Ö.; Foresman, J.B.; Ortiz, J.V.; Cioslowski, J.; Fox, D.J. Gaussian, Inc., Wallingford CT, **2009**.

23 Grimme, S.; Ehrlich, S.; Goerigk, L. *J. Comput. Chem.* **2011**, *32*, 1456-1465.

24 Grimme, S.; Steinmetz, M. *Phys. Chem. Chem. Phys.* **2013**, *15*, 16031.

25 Ryde, U.; Mata, R.; Grimme, S. *Dalton Trans.* **2011**, *40*, 11176.

26 Sun, Y.; Chen, H. *Journal of Chemical Theory and Computation* **2013**, *9*, 4735-4743.

27 Scalmani, G.; Frisch, M. *J. Chem. Phys.* **2010**, *132*, 114110.

28 Becke, A.; Edgecombe, K. *J. Chem. Phys.* **1990**, *92*, 5397-5403.

29 Silvi, B.; Savin, A. *Nature* **1994**, *371*, 683-686.

30 Savin, A.; Silvi, B.; Colonna, F. *Can. J. Chem.* **1996**, *74*, 1088-1096.

31 Bader, R.; Nguyen-Dang, T. *Adv. Quantum Chem.* **1981**, 63-124.

32 Bader, R. *Monatsh. Chem.* **2005**, *136*, 819-854.

33 Noury, S.; Krokidis, X.; Fuster, F.; Silvi, B. *Comput. Chem.* **1999**, *23*, 597-604.

34 AIMAll (Version 17.11.14), Keith, T.; TK Gristmill Software, Overland Park KS, USA, **2017**

35 Glendening, E. D.; Badenhoop, J. K.; Reed, A. E.; Carpenter, J. E.; Bohmann, J. A.; Morales, C. M.; Landis, C. R.; Weinhold, F. **2013**, Natural bond orbital analysis program: NBO 6.0. *Theoretical Chemistry Institute, University of Wisconsin, Madison, WI*.

36 Purvis, G.; Bartlett, R. *J. Chem. Phys.* **1982**, *76*, 1910-1918.

37 Pople, J.; Head-Gordon, M.; Raghavachari, K. *J. Chem. Phys.* **1987**, *87*, 5968-5975.

38 Popelier, P.; Logothetis, G. *J. Organomet. Chem.* **1998**, *555*, 101-111.

39 Silvi, B. *J. Mol. Struct.* **2002**, *614*, 3-10.

40 Zins, E. L.; Silvi, B.; Alikhani, M. E. *Phys. Chem. Chem. Phys.* **2015**, *17*, 9258-9281.

41 Waterman, R. *Chem. Soc. Rev.* **2013**, *42*, 5629.

42 Epstein, L.; Shubina, E. *Coord. Chem. Rev.* **2002**, *231*, 165-181.

43 Safin, D. A.; Babashkina, M. G.; Robeyns, K.; Mitoraj, M. P.; Kubisiak, P.; Garcia, Y. *Chem. Eur. J.* **2015**, *21*, 16679-16687.

44 Wolstenholme, D. J.; Traboulsee, K. T.; Hua, Y.; Calhoun, L. A.; McGrady, G. S. *Chem. Commun.* **2012**, *48*, 2597-2599.

45 Wolstenholme, D. J.; Dobson, J. L.; McGrady, G. S. *Dalton Trans.* **2015**, *44*, 9718-9731.

46 Glendening, E.; Landis, C.; Weinhold, F. *Wiley Interdiscip. Rev. Comput. Mol. Sci.* **2011**, *2*, 1-42.